Atmos. Chem. Phys. Discuss., https://doi.org/10.5194/acp-2018-1217
Manuscript under review for journal Atmos. Chem. Phys.
Discussion started: 26 November 2018

Atmospheric Chemistry and Physics
Open Access
EGU
Discussions

Assessment of the theoretical limit in instrumental detectability of Arctic methane sources using ^{13}C atmospheric signal

Thibaud Thonat[1], Marielle Saunois[1], Isabelle Pison[1], Antoine Berchet[1], Thomas Hocking[1], Brett Thornton[2], Patrick Crill[2] and Philippe Bousquet[1]

[1] Laboratoire des Sciences du Climat et de l'Environnement, LSCE/IPSL, CEA-CNRS-UVSQ, Université Paris-Saclay, F-91191 Gif-sur-Yvette, France
[2] Department of Geological Sciences and Bolin Centre for Climate Research, Svante Arrhenius väg 8, 106 91, Stockholm, Sweden

Abstract.
Despite their modest 4% magnitude compared to global emissions, Arctic methane sources are key elements in closing the global atmospheric methane budget, due to high uncertainties in their quantification and to their strong climate sensitivity. Recent efforts brought together bottom-up quantification approaches (inventories, process-based models) and regional observations of methane concentrations through inverse modelling to better estimate the Arctic methane sources, but the relatively small number of available observations in Arctic regions leaves gaps in fully understanding the drivers and distributions of the different types of methane sources present in the Arctic. Observations of methane isotope ratios could bring new insights on methane processes with increasingly affordable and accurate instruments. Here, we present the source signal that could be observed from methane isotopic measurements if high-resolution observations were available, and thus what requirements should be fulfilled in future instrument deployments in terms of accuracy in order to constrain different emission categories. This theoretical study uses the regional chemistry-transport model CHIMERE driven by different scenarios of isotopic signatures for each regional methane source mix. It is found that if the current network of methane monitoring sites is equipped with instruments measuring the isotopic signal continuously, only sites that are significantly influenced by emission sources could differentiate regional emissions from the background with a reasonable level of confidence. Nevertheless, we show that the detection of individual Arctic sources requires daily accuracies of <0.5‰, <0.2‰, <0.15‰, and <0.1‰ for wetlands, freshwaters, ESAS, and anthropogenic Arctic emissions, respectively, although these limits vary considerably depending on the observational site.

1 Introduction

Atmospheric methane (CH_4) is a potent climate forcing gas, responsible for more than 20% of the direct additional radiative forcing caused by human activities since pre-industrial times (Ciais et al., 2013). After staying nearly constant between 1999 and 2006, methane concentrations have been increasing again (Dlugokencky et al., 2011; Saunois et al., 2016). The explanations of this renewed accumulation are still widely debated. Recent studies, however, stress the major role played by microbial sources, particularly in the tropics (Schaeffer et al., 2016; Nisbet et al., 2016; McNorton et al., 2016; Saunois et al., 2017) together with uncertain contributions of fossil-fuel-related emissions (Schwietzke et al., 2017; Saunois et al., 2016) associated with a probable decrease in biomass burning emissions (Worden et al., 2018). Decreases in atmospheric sinks (Rigby et al., 2017; Turner et al., 2016) have also been postulated to contribute to the rise, though changes in methane sink cannot explain this rise by themselves.

Although the Arctic (>60°N) represents only about 4% of global methane emissions (Saunois et al., 2016) and does not seem to be a main contributor to the increasing trend of the past decade (e.g. Nisbet et al., 2018), it is a region of major interest in the context of climate change. The Arctic is particularly sensitive to climate driven feedbacks. For instance, higher temperatures may favour methane production from wetlands and methane release from thawing permafrost as protected carbon becomes available to remineralization to drive a sustained carbon feedback to climate change (Schuur et al., 2015). Most major source types for methane are present in the Arctic: natural wetlands, gas industry, and peat and forest burnings. There are also two types of sources that have received an increasing attention this past decade: freshwater systems (Walter et al., 2007; Bastviken et al., 2011; Tan and Zhuang, 2015; Wik et al., 2016) and subsea permafrost and hydrates in the East Siberian Arctic Shelf (ESAS, in the Laptev and East Siberian Seas; Shakhova et al., 2010; Berchet et al., 2016; Thornton et al., 2016a).

Methane sources and sinks can be estimated by a variety of approaches generally classified as either top-down (driven by atmospheric transport and concentration data) or bottom-up (driven by inventories and process-based models; e.g. Saunois et al., 2016). Our understanding of the methane global budget and its evolution is limited by the uncertainties about sources (their location, intensity, seasonality and proper classification) and sinks, by the representative coverage of the current observational surface network, by the biases of satellite-based data (e.g.

Atmos. Chem. Phys. Discuss., https://doi.org/10.5194/acp-2018-1217
Manuscript under review for journal Atmos. Chem. Phys.
Discussion started: 26 November 2018

Bousquet et al., 2018) and by the quality of atmospheric transport models (e.g. Patra et al., 2018). In particular, the discrepancies between bottom-up and top-down estimates remain a major concern both globally (Saunois et al., 2016) and in the Arctic (Thornton et al., 2016b; Thompson et al., 2017). Methane sources are particularly numerous, and temporally and spatially variable especially when compared to carbon dioxide's. This presents challenges in allocating the emissions to the particular sources as illustrated in Berchet et al. (2015), who studied overlapping wetland and anthropogenic emissions in Siberian lowlands. Improving the attribution of methane emissions to specific processes can benefit from the additional information provided by the ratios of stable isotopes in atmospheric methane concentrations.

There are respectively three main stable isotopologues of methane that are commonly measured, $^{12}CH_4$, $^{13}CH_4$ and $^{12}CH_3D$. Their respective abundances in the atmosphere are approximately 98.8%, 1.1% and 0.06% (Bernard, 2004). An isotopic signature characterizes each source and sink. The fractionation between the different isotopes is driven by source and sink processes that vary in space and time (Schwietzke et al., 2017). Microbial sources produce methane depleted in heavy isotopes. The isotopic signatures of biological sources vary depending on the metabolic pathway of formation, the nature of the degraded organic matter, on its stage of degradation, and on temperature (Whiticar, 1999). Thermogenic sources related to fossil fuels emit methane that tends to be not as depleted in heavy isotopes as microbial sources. Pyrogenic sources related to incomplete biomass combustion are even less depleted, with combustion of C3 plants contributing lighter signatures than C4 plants. Sink processes also influence methane's isotopic composition. The isotopic fractionations associated with both reaction with OH and uptake by soils, enrich atmospheric methane in heavier isotopes compared to the mean source signature. Atmospheric methane carries the isotopic signature resulting from the summed value of all of its sources and sinks. In this study, only $^{12}CH_4$ and $^{13}CH_4$ are considered.

The isotopic variations are small: the ratio of $^{13}C/^{12}C$ in methane is expressed in conventional delta notation as $\delta^{13}C\text{-}CH_4$, which is the part per thousand deviation of the ratio in a sample to that in an international standard:

$$\delta^{13}C\text{-}CH_4 = [(R_{sample} / R_{standard}) - 1)] \times 1000\ ‰ \qquad (1)$$

where R is $^{13}C/^{12}C$ of either the sample or of a community determined standard (currently Vienna-Pee Dee Belemnite, V-PDB; Craig, 1957).

The use of stable isotopes for discriminating methane sources is not new (Schoell, 1980). Isotope data can bring a valuable constraint on the methane budget (Mikaloff-Fletcher et al., 2004) and be relevant to eliminate different emission scenarios used to explain methane evolutions, globally (Monteil et al., 2011; Saunois et al., 2017) or regionally, for example in the Arctic (Warwick et al., 2016). Since 2007, globally averaged atmospheric methane concentrations have been steadily increasing and at the same time it has become more depleted in ^{13}C. Nisbet et al. (2016) found the post-2007 shift in the $\delta^{13}C\text{-}CH_4$ value of the global atmospheric mean concentration to be -0.17‰. This shift signifies major on-going changes in the methane budget and can be used to bring additional constraints on the source partitioning (Saunois et al., 2017). Using a box-model, Schaeffer et al. (2016) estimated the $\delta^{13}C\text{-}CH_4$ value of the post-2007 globally averaged source needed to match the observed $\delta^{13}C\text{-}CH_4$ evolution, to be -59‰. They concluded that the post-2007 rise was driven by microbial emissions, in particular from agricultural sources. The Schaeffer et al. (2016) estimate was used to validate the sectoral partition of the emission changes for 2000-2012 retrieved by Saunois et al. (2017). However, large uncertainties remain for source signatures, implying that $\delta^{13}C\text{-}CH_4$ cannot point towards a unique solution.

Three main limitations remain in the use of isotopic data to improve our knowledge of methane sources and sinks: the wide ranges of isotopic signatures, the lack of information to estimate these signatures, and the lack of atmospheric isotopic data to assimilate in top-down approaches (Tans, 1997).

Isotopic signatures span large ranges of values, typical ranges being -70 to -55‰ for microbial, -55 to -25‰ for thermogenic and -25 to -13‰ for pyrogenic sources (Kirschke et al, 2013). Actually, significant overlap occurs (see Thornton et al., 2016b, and Section 2.4: e.g. -110 to -50‰ for microbial signatures, -80 to -17‰ for coalfields). Modelling studies do not always reflect these ranges because they choose only one or a few values for each source. McCalley et al. (2014) found that using the commonly used isotopic signature for wetlands for future emissions related to thawing permafrost could entail overestimations of a few $TgCH_4$ and an erroneous source apportionment. Recently, Sherwood et al. (2017) compiled a global comprehensive database of $\delta^{13}C\text{-}CH_4$ and other methane isotopic signatures for fossil fuel, microbial and biomass burning sources. They pointed out that most modelling studies relied on a set of canonical isotopic signature values that circulated within the modelling community, which could have led to the use of erroneous values. For example, using a previous version of this database, Schwietzke et al. (2016) revised the fossil fuel methane emissions upward by about 50% for the past three decades.

The lack of information on $\delta^{13}C$-CH_4 signatures is also a limitation for identifying sources of distinctive methane plumes (France et al., 2016). However, several recent measurement campaigns showed the value of determining $\delta^{13}C$-CH_4 for source apportionment. For example, the isotopic analyses led by Cain et al. (2016) from aircraft data in the North Sea made it possible to identify a source in a plume downwind of gas fields, which would have been missed without it. In the Arctic, the importance of wetland emissions has been highlighted with the analysis of isotopic data from aircraft, ships and surface stations (Fisher et al., 2011; O'Shea et al., 2014; France et al., 2016). Field campaigns are also regularly organized to measure the isotopic signatures of various sources (Pisso et al., 2016; McCalley et al., 2014; Fisher et al., 2017).

The paucity of isotopic measurements to constrain top-down atmospheric inversions is another limitation. Inversions assimilating both total methane and isotope data are few; they use only flask sampling data, and rely on a few sites around the world. This, together with the lack of information on isotopic signatures can explain why such multi-constraint inversions have mostly been conducted with simple box-models so far (e.g. Schaefer et al., 2016). However, laser spectrometers can now provide continuous observations of methane isotopes with permanently increasing performances (Santoni et al., 2012). Moreover, such high frequency and high precision isotope measurements were shown, if applied to the current observational network, to potentially add significant certainty to source inversion in all sectors, even at the national scale (Rigby et al., 2012).

Even though no long-term continuous atmospheric ^{13}C time series are yet available, it seems important to evaluate their potential to improve our knowledge on methane sources and sinks. A first step is the modelling of the isotopic signals to be expected at possible monitoring sites due to the different sources, taking into account the range of isotopic signatures. The Arctic region is chosen as a test region because of the significant potential of the climate-carbon feedback mentioned earlier and because methane emissions may overlap less (in time and space) than in the tropics for instance.

Following Thonat et al. (2017), who estimated the detectability of methane emissions at Arctic sites measuring total CH_4, this paper aims at extending this approach to $\delta^{13}C$-CH_4 observations, even if they do not exist yet. After presenting the 24 existing monitoring sites in the Arctic and the modelling framework (section 2), we evaluate how well our model simulates $\delta^{13}C$-CH_4 at the five sites where it is already monitored (section 3.1). Then, the atmospheric signals of the various Arctic methane sources at these sites are estimated (section 3.2) before determining their detectability based on instrumental constraints and on the uncertainties of the isotopic signatures (section 3.3).

2 Measurements and modelling framework

2.1. Measurements

Measurements of the isotopic ratio in atmospheric methane for 2012 come from five Arctic surface sites (White et al., 2018). The locations of these sites are shown in Fig. 1 and their characteristics are given in Table 1. Most of them are considered to be sampling background air: Alert is located in North Canada; Zeppelin (Ny-Ålesund) is on a mountaintop in the Svalbard archipelago; Cold Bay is in the Alaska Peninsula; and Summit is at the top of the Greenland Ice Sheet. The Barrow observatory, located in the North Slope of Alaska, is more affected by local wetland emissions. NOAA-Earth System Research Laboratory (NOAA-ESRL) is responsible for the collection and analysis of the weekly flask samples. The isotopic composition is determined by INSTAAR (Institute of Arctic and Alpine Research) of the University of Colorado. All data are reported in conventional delta notation, in per mil (‰). The $\delta^{13}C$-CH_4 observations are given with a precision of better than 0.1‰ (White et al., 2018). All data without reported issues in collection or analyses are selected; outliers above 3-sigma of the variability at the station are discarded.

Other sites where atmospheric methane is measured are also included in this study. They do not provide $\delta^{13}C$-CH_4 observations, but we evaluate their potential in doing so. Their description is given in Table 1 as well.

2.2 Model description

The Eulerian chemistry-transport model CHIMERE (Vautard et al., 2001; Menut et al., 2013) is used to simulate tropospheric $^{12}CH_4$ and $^{13}CH_4$ concentrations separately, the isotope ratio being computed offline a posteriori. Following Thonat et al. (2017), the domain has a regular kilometric resolution of 35 km, which avoids numerical issues due to too small grid cells close to the Pole encountered in regular latitude-longitude grids. It covers all longitudes above 64°N but can extend to 39°N, as illustrated in Fig. 1. The troposphere is divided into 29 vertical levels from the surface to 300 hPa (~9000 m).

CHIMERE solves the advection-diffusion equation, forced using meteorological fields from the ECMWF (European Centre for Medium Range Weather Forecasts, http://www.ecmwf.int/) forecasts and reanalyses. Wind, temperature, water vapour and other meteorological variables are given with a 3 h time resolution, at ~0.5° spatial resolution, and 70 vertical levels in the troposphere. Initial and boundary concentrations of $^{12}CH_4$ and $^{13}CH_4$ come from global simulations of the general circulation model LMDZ (Hourdin et al., 2006) for the year 2012. These fields have a 3 h time resolution and 3.75°x1.875° spatial resolution. All these fields are interpolated in time and space within the grid of the CHIMERE domain.

The model is run with various tracers, each one corresponding either to the $^{12}CH_4$ or to the $^{13}CH_4$ component of a methane source. Simulated $^{12}CH_4$ and $^{13}CH_4$ of all sources are then used in the calculation of $\delta^{13}C\text{-}CH_4$. This allows us to analyse the contribution of each source in $\delta^{13}C\text{-}CH_4$. Three pairs of tracers correspond to anthropogenic sources: emissions from oil and gas; from solid fuels (coal); and other anthropogenic emissions (mostly from enteric fermentation and solid waste disposal). One pair of tracers corresponds to biomass burning. Two pairs correspond to geological sources: continental micro- and macro-seepages; and marine seepages. Three pairs correspond to other natural sources: wetlands, freshwater systems, and emissions from the ESAS. Another pair of tracers corresponds to soil uptake, considered as a negative source. Finally, one pair of tracers corresponds to the boundary conditions. No chemistry is included in the multi-tracers simulation, but another simulation is done including the reaction with OH in order to assess the contribution of this major sink.

In this study, simulations were run for the year 2012. With the chosen model set-up spanning Arctic regions, the typical mixing time of air masses in the domain is 2-4 weeks. Therefore, simulations in January are partly influenced by prescribed initial conditions from global fields during the spin up period. This has little impact on our conclusions because CH_4 emissions are relatively limited in winter in the Arctic.

2.3 Input emission data

Surface emissions used as inputs in the model come from various inventories, models, and data-driven studies. The emissions used are described and discussed in more details in Thonat et al. (2017) and summarized below and in Table 2.

All anthropogenic emissions are taken from the EDGARv4.2FT2010 yearly product (Olivier and Janssens-Maenhout, 2012). When possible, the 2010 data are updated using FAO (Food and Agriculture Organization, http://www.fao.org/faostat/en/#data/) and BP (http://www.bp.com/) statistics (on enteric fermentation, and manure management, and on oil and gas production, fugitive from solid, respectively). For 2012, anthropogenic emissions amount to 20.5 $TgCH_4\ yr^{-1}$ in our domain, mostly from the fossil fuel industry. Biomass burning emissions come from the GFED4.1 (van der Werf et al., 2010; Giglio et al., 2013) monthly product, and represent 3.1 $TgCH_4\ yr^{-1}$ in our domain.

Wetland emissions are derived from the ORCHIDEE global vegetation model (Ringeval et al., 2010, 2011), on a monthly basis. Annual emissions from wetlands in our domain correspond to 29.5 $TgCH_4\ yr^{-1}$. A large uncertainty affects wetland emissions, which can vary widely depending on the chosen land vegetation model and wetland area dynamics (e.g., Bohn et al., 2015). Emissions from geological sources stem from the GLOCOS database (Etiope, 2015), and amount to 4.0 $TgCH_4\ yr^{-1}$ in our domain. ESAS emissions are prescribed to 2 $TgCH_4\ yr^{-1}$, in agreement with the estimate made by Thornton et al. (2016) based on a ship measurement campaign, and with the estimate made by Berchet et al. (2016) based on atmospheric observations at surface stations. The temporal and geographic variability of the ESAS emissions is based on the description by Shakhova et al. (2010), following the modelling framework of Berchet et al. (2016).

A total value of 15 $TgCH_4\ yr^{-1}$ was prescribed for all lakes and reservoirs located at latitudes above 50°N. The localisation of freshwater systems relies on the GLWD level 3 map (Lehner and Döll, 2004). Our inventory was built based on some simplifications: the emissions are uniformly distributed among lakes and reservoirs; no emission occurs when the lake is frozen, and emissions are constant otherwise. Freeze-up and ice-out dates are estimated based on surface temperature data from ECMWF ERA-I reanalyses. Freshwater emissions amount to 9.3 $TgCH_4\ yr^{-1}$ in our domain, which is consistent with recent pan-Arctic studies (e.g., Wik et al., 2016; Tan and Zhuang, 2015).

Atmos. Chem. Phys. Discuss., https://doi.org/10.5194/acp-2018-1217
Manuscript under review for journal Atmos. Chem. Phys.
Discussion started: 26 November 2018

Atmospheric Chemistry and Physics
Open Access
Discussions

2.4 Source isotopic signatures

Source signatures are chosen constant in time and space in our modelling framework. Regional seasonal variations of microbial signatures are expected to be small (e.g. Sriskantharajah et al., 2012); some homogeneity can be assumed at the scale of our domain, which only comprises high northern latitudes; and possible heterogeneity is assumed to be smoothed out by the model 35 km horizontal resolution. The representativeness of each reported signature is different, so that using regional means may avoid giving too much weight to outliers. Also, considering that most atmospheric sites are located far from large emission areas, the signals in the emissions are mixed by the atmospheric transport. Therefore, we have chosen to use only one value for each source but to test various scenarios with different isotopic signatures (see Sect. 3.2).

The Sherwood et al. (2017) data on fossil fuel emissions for countries within our domain show a wide range of measured isotopic signatures. For conventional gas and shale gas, data range between -76 and -24‰, with means, for Russia (number of data, n=556), Canada (n=490), Norway (n=28), and the US (Alaska) (n=20), of -46, -51, -44, and -43 ‰ respectively. Heavier signatures (typically -40‰) are generally used for oil and gas related emissions in global studies (e.g. Houweling et al., 2006; Lassey et al., 2007) and for Arctic studies as well (Warwick et al., 2016), but more depleted signatures have also been used for Russia (-50‰ in Levin et al., 1999). Given that Russia is by far the largest emitter of methane from natural gas production and distribution, we chose here the value of -46‰ for the whole domain. As it is difficult to distinguish between methane associated to gas and oil exploitation, the same signature is used for both.

The range of isotopic values is also very large for emissions from coalfields: from -80 to -17‰ (Rice, 1993). Data are scarcer in the Sherwood et al. (2017) database than for natural gas, with just one reference for Russia and 92 reported values for Canada, the mean being -55‰. Russia is again the top emitter in this category, but the paucity of the data prevents us from using the single value for the whole domain. Zazzeri et al. (2016) highlighted the dependence of the isotopic value on the coal rank and type of mining, although national and regional specificities remain. Basically, the higher the coal rank (i.e. the carbon content), the heavier the isotopic signature. The main Russian coal basins, the Kuznetsk and Kansk-Achinsk basins, located in southern Siberia, where low rank coal is extracted, are not part of our domain. The few major hotspots of emission associated to coal in our domain, according to EDGARv4.2FT2020, correspond to basins where hard coal is exploited, and mainly bituminous coal (Podbaronova, 2010). According to the broad classification suggested by Zazzeri et al. (2016) for modellers, this means rather light isotopic signatures, between -55 and -65‰. Consequently, we choose -55‰ for emissions associated to coal in our domain, which is lighter than the values usually used in global methane budgets (e.g. -37‰ in Bousquet et al. (2006) and Tyler et al. (2007); -35‰ in Monteil et al. (2011)).

Other non-negligible anthropogenic sectors in our domain are enteric fermentation and waste disposal. For the former, the $\delta^{13}C$ signature depends strongly on the ruminants' diet and on the species. Klevenhusen et al. (2010) found signatures from cows of -68‰ or -57‰, depending on the diet, in agreement with previous studies by Levin et al. (1993) and Bilek et al. (2001). Here, a value of -62‰ was used, as in other methane isotopic budgets (e.g. Tyler et al., 2007; Monteil et al., 2011). Methane emitted by organic waste is enriched as a result of methane oxidation after its production in the anoxic layer. Here, a value of -52‰ was used, in agreement with Chanton et al. (1999) (-58 to -49‰) and close to what was found by Bergamaschi et al. (1998b) (-55‰).

Walter Anthony et al. (2012) found natural seeps concentrated along the boundaries of permafrost thaw and retreating glaciers in Alaska and Greenland, with a wide range of isotopic signatures, originating from fossil and also younger methane. However, geological methane is mostly of thermogenic origin (Etiope, 2009), and this is also true for submarine seepage (e.g. Brunskill et al., 2011). As a consequence, the isotopic signature used here for geological methane, both continental and submarine, is -49‰, following Etiope (2015), close to oil and gas methane signatures.

The values of isotopic signatures for biomass burning are found in a small range, despite their dependency on the fuel type and the combustion efficiency. For example, Chanton et al. (2000) reported values comprised between -30‰ and -21‰ for US forests. Yamada et al. (2006) estimated the global biomass burning $\delta^{13}C$-CH_4 at -24‰, while Whiticar and Schaefer (2007) suggested -25‰. Here, the value of -24‰ was used.

Microbial methane from wetlands has a wide range of isotopic signatures, varying from -110 to -50‰ (Whiticar, 1999). Acetoclastic fermentation results in methane relatively less depleted in ^{13}C ($\delta^{13}C$-CH_4 of -65 to -50‰), while CO_2 reduction produces methane highly depleted in ^{13}C ($\delta^{13}C$-CH_4 of -110 to -60‰) (Whiticar, 1999; McCalley et al. 2014). The partition between these two production pathways depends partly on the ecosystem

Atmos. Chem. Phys. Discuss., https://doi.org/10.5194/acp-2018-1217
Manuscript under review for journal Atmos. Chem. Phys.
Discussion started: 26 November 2018

Atmospheric Chemistry and Physics
Discussions

type and season. The isotopic signature of the emitted methane also depends on other factors, such as the pathways of transport and oxidation (Chasar et al., 2000). Several studies on the isotopic signature of wetlands are compiled in Table 3, focusing on high northern latitudes. All studies report values generally ranging between -75‰ and -60‰. Here again, the difficulty in dealing with these reported source signatures has to do with their representativity. Some observations are from chamber studies, which, by nature, focus on very local signals; others are given by ambient air samplings and can be representative of several hundred square kilometres, so possibly encompassing other source and sink determinants. The chamber studies present a wide variety of values for the same site. For example, Fisher et al. (2017) reported values at the Stordalen Mire ranging from -112 to -48‰; even in the same week, changes can be as large as 30‰. The signals can also vary significantly with the time of year and the kind of ecosystem (McCalley et al., 2014). For example, for three different peatland systems in Finland, Galand et al. (2010) report values that differed by 30‰. Consequently, values in Table 3 are mostly derived from ambient air samplings rather than chamber measurements, and we give means rather than the whole measured ranges. The value of -70‰ was used in our study, close to the recommendation to modellers made by Fisher et al. (2017) (-71 ± 1‰) and France et al. (2016) for wetlands above 60°N.

Most values labelled "Wetlands" in Table 3 encompass not only wetlands but also a mix of wetlands and other exposed freshwater systems. Shallow lakes, ponds and pools, common in the Arctic, have not always been considered a distinct source (Bastviken et al., 2011). This is another limitation in estimating the global methane budget (Saunois et al., 2016). Signature estimates based on air sampling are representative of a wide area, where exposed freshwaters are undoubtedly present. Moreover, signature ranges reported specifically from Arctic lakes are not precise enough to distinguish between water body types, and overlap those of wetlands (Wik, 2016). In the range of recent reported values (Walter et al., 2008; Brosius et al., 2012; Bouchard et al., 2015; Wik, 2016; Thompson et al., 2016), and close to the value used for Arctic wetlands, the value of -66‰ was used for the isotopic signature of freshwater system emissions in our domain.

Sources of methane in the ESAS are varied and it is still a challenge to determine the origin of methane produced and emitted there (Ruppel, 2015). The shallow ESAS is underlain by formerly subaerial permafrost that has been flooded by sea level rise since the Pleistocene (Dmitrenko et al., 2011). Carbon can be released via the degradation of permafrost or decomposition of gas hydrates. Sapart et al. (2017) showed that sediments in ESAS have isotopic signatures ranging between the two main microbial methane formation pathways. An earlier study, Cramer and Franke (2005), observed significantly heavier CH_4 ($\delta^{13}C$-CH_4 ~-39.9 per mille) in Laptev Sea near-surface sediments, attributed to a deep thermogenic source. A wider range, with much lighter CH_4 was detected in the Laptev seawater column. Methane in the water is more enriched in ^{13}C than in sediments, but the emitted methane signature is in the range of wetland emissions. Based on fewer data than Sapart et al. (2017), Overduin et al. (2015) reported more positive values, associated to strong ^{13}C enrichment in the upper thawed permafrost layers. A signature of -58‰ was used here for emissions from ESAS, in the range of the literature.

2.5 Sinks: isotopic fractionation

The main sinks of methane in the troposphere are its oxidation by hydroxyl radicals (OH), which accounts for about 90% of the total sink (Saunois et al., 2016), its reaction with chlorine (Cl) in the marine boundary layer (about 3%) and its uptake by soils (about 3%, at the global scale; Kirshke et al., 2013). Methane uptake occurs in unsaturated oxic soils due to the presence of methanotrophic bacteria. This sink may be particularly important in the high latitude region with wetlands. In our domain of simulation, its magnitude is equal to biomass burning emissions in absolute value. Oxidation in marine systems can also be coupled to sulfate reduction as well in sub-oxic environments. This will not affect the atmospheric values directly but will shift the source signatures of the methane that is emitted from the surface to heavier values after having been diffusively advected from its sedimentary sites of production through the water column to the atmosphere.

Due to the difference in mass between the $^{12}CH_4$ and $^{13}CH_4$ isotopologues, chemical reactions in the atmosphere preferentially consume the lighter isotopologue, potentially causing significant fractionation. This is another reason why the $\delta^{13}C$ of methane in the atmosphere is not the same as that of the total source. Sinks can be characterised by their kinetic isotope effect (KIE), the ratio of the reaction rate coefficients (k) for two different isotopologues of the same molecule: k_{light}/k_{heavy}. For the reaction with OH this value is 1.0039 (Saueressig et al., 2001). For the soil uptake, the KIE is 1.020, which is represented by a fixed $\delta^{13}C$-CH_4 source signature of -65.7‰ in our model set-up.

3 Results

Simulations of distinct tracers, each one corresponding to a different $^{12}CH_4$ or $^{13}CH_4$ source, are run with CHIMERE for the year 2012. Since isotopic signatures generally vary over a wide range for a given source, we ran simulations using the mean value and the extreme values of the range given in Table 2 for wetland, freshwater and ESAS emissions. The boundary conditions are the dominant signal in our domain, especially in winter, both in terms of total methane mixing ratio (in ppb) and $\delta^{13}C$-CH_4 value (in ‰), as illustrated in Figure 2. The boundary conditions represent methane coming from lower latitudes south of the Arctic domain (Fig. 1). They cannot be considered as a background level of methane given that (i) they may be due to emissions from the Arctic that have left our domain and then re-entered it; (ii) they may bring to the domain air masses that are particularly depleted or enriched in methane. However, they are excluded from our analysis to only focus on the direct contribution of sources located within the Arctic domain.

3.1 Comparison between modelled and observed $\delta^{13}C$-CH_4

Most of the five sites where weekly $\delta^{13}C$-CH_4 measurements are available are remote from any emitting areas (Fig. 1), with the exception of Barrow where significant methane enhancements from nearby wetlands can happen in summer (Sweeney et al., 2016). For most remote sites, the maximum $\delta^{13}C$-CH_4 is reached in May-June and ranges between -47.3 and -47.1‰ (Fig. 2). Then wetlands and freshwater systems start emitting ^{13}C-depleted methane and the minimum is reached in September-early November, with values around -47.8‰. One exception is Cold Bay where $\delta^{13}C$-CH_4 in January was much lower than other sites. In Barrow, the minimum reaches -48.2‰. The yearly mean is -47.6‰ at Barrow and -47.5‰ at the other sites. The seasonal amplitude is about 0.6‰. The variability of the measurements is higher in Barrow and Cold Bay compared to the three others, highlighting that these two sites are the most sensitive to Arctic sources at the synoptic scale.

The contribution of the boundary conditions to simulated $\delta^{13}C$-CH_4 is approximately between -47.2 and -47.6‰. The increment added by Arctic sources lies between -0.1 and -0.2‰ in summer (June-October), except in Barrow where it is -0.4‰, and is close to zero in winter (November-May). On a yearly basis, our model overestimates $\delta^{13}C$-CH_4. The large overestimation in winter (~0.2‰) is due to the boundary conditions that are too high in terms of total methane compared to continuous measurements (as shown in Thonat et al., 2017). Too large contribution of low latitude fossil sources leads to higher $\delta^{13}C$-CH_4 values. Nevertheless, large depleted peaks can be observed in winter at Barrow and Alert, which can be attributed to ESAS emissions. With a reference ESAS emission signature of -58‰, the magnitude of most of these peaks are under-estimated by the model, pointing at either an under-estimated total methane contribution, or an under-estimated isotopic depletion in the source. In summer, the model underestimates $\delta^{13}C$-CH_4 by less than 0.11‰ at all sites, which is in the range of the uncertainty of the measurements. However, the seasonality is only fairly captured by the model. The decrease in early summer comes too soon and so does the autumn minimum. Thonat et al. (2017) demonstrated that this result is mostly emission-driven: the seasonality of wetland emissions is not well reproduced by the various existing land surface models. Wetland emissions derived from biogeochemical models occur too soon and cover too short a period during the year, which can explain some of the discrepancies observed here between the model and the observations.

Despite their importance to assess the inter-annual variability and seasonality of $\delta^{13}C$-CH_4, the available flask measurements do not allow us to quantify the ability of the model to represent the synoptic variations. Continuous measurements of $\delta^{13}C$-CH_4 would be necessary to evaluate the model in a more quantitative way. Even though further improvements will be necessary in the model, we assume in the following that the model performances associated to sensitivity tests using various isotopic signatures are sufficient for estimating the magnitude of the isotopic signals originating from the various Arctic sources.

3.2 Contributions of Arctic sources in $\delta^{13}C$-CH_4 at Arctic sites

In terms of total methane, our domain is dominated by anthropogenic sources in winter, and by wetland emissions in summer. ESAS and geological sources can also have a relatively significant impact in winter in some areas, while freshwater systems are an important contributor to atmospheric methane in summer (Thonat et al., 2017). The spatial distribution of the source contribution to the $\delta^{13}C$-CH_4 value depends on the magnitude of the emission but also on the difference between the isotopic signature of the source and of the boundary conditions. The difference between total $\delta^{13}C$-CH_4 and the contribution of the boundary conditions (Figure 2, black and cyan lines, respectively) represents the sum of the direct contribution from the various Arctic sources at the measurement locations. The combination of the various signals due to Arctic sources depends on the station, as shown in Fig. 2.

These five sites do not form a large-enough sample to be representative of all Arctic sites. Therefore, Figure 3 shows the winter and summer means of the simulated direct contributions of the various Arctic sources to the δ^{13}C-CH_4 value at the 24 sites of Fig. 1. For each site, the contribution of each source is plotted along a cumulative dotted line. The rightmost black point of each line represents the total contribution of all Arctic sources i.e. the difference between simulated total δ^{13}C-CH_4 and δ^{13}C-CH_4 from the boundary conditions alone. The bars indicate, by their colours and by their position (at 0.1 ‰ resolution in winter; 0.5 ‰ resolution in summer), the proportion of days in the season when a given range of the total contribution of all Arctic sources in δ^{13}C-CH_4 values is reached. Time resolution is 1 day. For example, if we consider TIK in winter: the direct contribution of all Arctic sources is -0.09‰ on average over the season. Over the whole winter, this contribution ranges between 0 and 0.1‰ less than 20% of the time; between 0 and -0.1‰ during 60-80% of the time; between -0.1‰ and -0.2‰ during 20-40% of the time; between -0.2‰ and -0.3‰ less than 20% of the time; and less than -0.3‰ for less than 20% of the time.

On average, the contributions of Arctic sources to the isotope ratio are very low in winter at all sites, between -0.12 and +0.03‰. The isotope ratio signal is low in winter because the largest contribution of Arctic sources to atmospheric methane in this season is due to oil and gas emissions, whose signature (-46‰) is very close to that of boundary conditions. One exception is YAK, where the mean Arctic contribution to δ^{13}C-CH_4 is -0.51‰. This is due to large simulated mixing ratios of methane from nearby coal emissions. The daily isotope ratio signal shift due to Arctic contributions there can reach -1.75‰. Geological emissions have a signature close to oil and gas in our modelling framework and do not show up from the simulated signal. On the contrary, ESAS emissions have an impact in terms of δ^{13}C-CH_4 at some sites at the synoptic scale: the maximum δ^{13}C-CH_4 Arctic contribution at AMB and CHS in winter is ~-0.5‰, and ~-0.4‰ at TIK, which are close to the shores of ESAS. NOY is the only site with a positive mean contribution to δ^{13}C-CH_4 in winter. Large enhancements of $^{12}CH_4$ from oil and gas, which in NOY regularly exceeds 100 ppb in winter, succeed in making a significant difference with the δ^{13}C-CH_4 value of the boundary conditions. Apart from NOY, the Arctic contribution to δ^{13}C-CH_4 is very rarely positive among the sites, and stays low when it is positive (maximum is 0.13‰ at DEM).

Compared to winter, higher contributions of Arctic sources to the δ^{13}C-CH_4 values are found in summer at most stations because of the large magnitude of natural emissions, especially from wetlands. Wetland emissions contribute more than two third of the signal at all sites, except BKL and CBB where the contribution of freshwater systems is also important, and YAK (again due to coal emissions). Wetlands keep the isotope ratio quite low, with four sites having a mean δ^{13}C-CH_4 contribution less than -1.0‰ (INU, BCK, NOY, CHS). Values below -2.0‰ are even reached on a daily basis at 15 sites; it is frequent at BCK for example, where the influence of wetlands and freshwater systems are combined. On top of wetland and freshwater influences, ESAS explains more than 10% of the signal at TIK and AMB.

Figure 3 reveals what can be expected on a seasonal basis at the different sites, but does not show how the various source contributions combine all along the year and how different source signatures can affect the total δ^{13}C-CH_4 signal. Figure 4 and the supplementary figures S1-S23 show the time series of the direct contribution of each source and sink to the total δ^{13}C-CH_4 at the 24 Arctic stations. A focus is put on Zeppelin station with Fig. 4 because a new Aerodyne instrument has been installed there during Summer 2018 to continuously measure δ^{13}C-CH_4 for at least one year. Figure 4 help showing the magnitude and timing of the maximum signal of each source during the year, the potential compensation between sources, and the seasonality of the various contributions.

Zeppelin is a rather simple case. δ^{13}C-CH_4 from anthropogenic emissions are very small (<0.02‰) and anyway tend to cancel out because (i) the source areas are far from the station and (ii) the signal from oil and gas, and from coal have approximately the same magnitude, but opposite signs. The signal from geological sources remains negligible. Only wetland emissions succeed to tear the signal away from the value of the boundary conditions, from June to October, with synoptic changes up to -0.2‰. Freshwater systems intensify the signal by 0.02‰ on average in summer, with maxima around 0.05‰ on a synoptic basis. But these contributions are diminished by biomass burning (~+0.01‰) and also by the fractionating effects of the two major sinks (~±0.01‰). The simulated Arctic δ^{13}C-CH_4 at the site is the result of these competing signals. Varying isotopic signatures of natural sources does not change the conclusions with wetland, freshwater and ESAS synoptic events reaching at maximum respectively -0.3‰, -0.1‰ and -0.15‰. Therefore, in the case of a remote station such as ZEP, individual signals remain below 0.3‰ on a synoptic scale and partial compensation between sources determines the total δ^{13}C-CH_4 anomaly.

Analysing other stations (Figures S1 to S23) reveals that synoptic events larger than 2‰ due to summer wetland emissions could happened at AMB, BEH, CHK, DEM, IGR, INU, NOY, TIK. For freshwater emissions, events larger than 0.5‰ are simulated at AMB, BKL, BMW, BEH, CAM, CHU, and INU. For ESAS, varying the isotopic signature induces synoptic events larger than 0.3‰ at some sites (AMB, BRW, CHK, TER, TIK). For anthropogenic emissions, only NOY shows synoptic events due to oil and gas that are larger than 0.15‰, and only YAK shows synoptic events due to fugitive emissions larger than 1‰; all these events occurring in winter. Biomass burning synoptic events are the largest at BEH, CAR, CHK, DEM, INU, KRS, NOY, and YAK with changes larger than 0.2‰.

The influence of the sinks on synoptic changes remains smaller than 0.05‰ at most sites. Note that the sink constituted by the reaction with Cl radicals in the marine boundary layer is not taken into account here, given its very small impact in our domain (Thonat et al., 2017), although it is highly fractionating.

3.3 Detectability of Arctic sources using isotopic measurements

The magnitude of Arctic $\delta^{13}C$-CH_4 signals to be expected at present and potential measurement sites and the contributions of individual sources to these signals do not lead directly to quantifying the detectability of individual sources, as the latter also depends on the performances of the measuring instrument. The flask measurements used here (Tab. 1, Fig. 1 and 2) have an uncertainty of about 0.1‰. They are obtained using GC-IRMS (gas chromatography isotope ratio mass spectrometry; White et al., 2018). Laser-based instruments, using Cavity Ring Down Spectrometry or direct absorption spectrometry (Nelson et al., 2004) have been developed for 10 years for CO_2 isotopes (McManus et al., 2010) and, more recently for methane (Santoni et al 2012). The Aerodyne QCL instrument has proven to be capable of high frequency (≥1 Hz) measurements of $^{12}CH_4$ and $^{13}CH_4$ isotopes of CH_4 with *in situ* 1 second RMS $\delta^{13}C_{CH4}$ precision of 1.5‰ and an Allan-minimum precision of 0.2‰ at 100 seconds (Santoni et al., 2012), recently improved to 0.1‰ through laser stability improvements. Such a small value (0.1 ‰) reaches the precisions reported for GC-IRMS (0.1‰). However, Aerodyne instruments face a strong drift that imposes a strict calibration protocol (every 2 hours in most recent set-ups), which dramatically reduces the daily number of available observations to typically a few tens. Considering that measurements are independent over the day, the expected precision on a daily average of N measurements is 0.1/sqrt(N) ‰, i.e. ~0.01-0.03 ‰.

In the following, we compare a range of expected instrument precisions to the Arctic source signals in order to determine the best site(s) to detect the various Arctic sources, taking into account the limitation brought by the uncertainties on the measurements. The range of uncertainties in the measuring instrument has been varied from an optimistic view (100 valid independent measurements per day with an individual uncertainty of 0.1‰ with no drift i.e. an uncertainty of 0.01‰ (= 0.1/sqrt(100)) for the daily mean) to a more pessimistic view (five valid independent measurements per day with a loose calibration procedure, leading to an individual uncertainty of 0.2‰ and a drift of 0.4‰ during the day, therefore a daily uncertainty of $0.5‰=\mathrm{sqrt}(0.4^2+(0.2/\mathrm{sqrt}(5))^2)$. We define a detectability threshold for a given source at a given site as follows: the simulated signal of total isotopic ratio must be larger than the instrument precision for at least 15 days in the year; then, if the given source is dominant in the simulated signal for more than 15 of these days, it is considered detectable. Detectability thresholds at the 24 sites of Table 1 are summarized in Table 4. We illustrate the estimation of the detectability of sources in Figure 5 for ZEP and Figures S24 to S46 for the other stations. At ZEP, with a 0.5‰ uncertainty, no source is detected, as the signal due to all Arctic sources is smaller than this threshold. If the measurement uncertainty reaches 0.1‰, wetland events may be detected during 130 days. Below 0.05‰ of measurement uncertainty, other sources might be detected. At only 0.01‰, there were 50 days of possible detection for ESAS, 20 days for freshwaters and less than 10 days for anthropogenic emissions. Taking into account all stations (Figures S24 to S46, and Table 4), wetland emissions are the most easily detected with more than 50 days for a measurement uncertainty above 0.2‰ for all sites but BKL, CBA, SUM, STO, VGN, and ZEP; the best scores of detection, with more than 150 days, are achieved at BEH, CHK, CAR, INU, DEM, NOY, and TIK. Freshwater emissions are easiest to detect at BKL and CAM with 100 days and 50 days above 0.2‰ respectively. Several other sites offer detection but with a more challenging threshold of 0.05‰ for the measurement uncertainty to get about 50 days of events (BEH, PAL, TER, VGN). For ESAS emissions, the minimum detection ranges in [0.02‰-0.5‰] depending on stations. ESAS emissions are best detected at AMB, CHK, and TIK with more than 50 days above 0.15‰, 0.15‰, and 0.1‰ respectively. A few other sites offer detectability if uncertainties are lower than 0.05‰ (ALT, CAM, BRW, INU, and ZOT). The minimum detection of ESAS emissions ranges in [<0.01‰-0.2‰] depending on stations. As already noticed, the effect of anthropogenic emissions dominates at YAK with about 100 days above 0.5‰ anomalies. Other sites show much less detectability with more than 50 days of events above 0.1‰ at NOY, and 0.02‰ at VGN. Without YAK, the minimum detection of anthropogenic emissions ranges in [<0.01‰-0.2‰] depending on stations. Other sources (biomass burning, geological leaks) remain mostly undetected with only a few days detected for uncertainties below 0.02‰ at YAK and VGN for biomass burning and ZOT for geological leaks.

4 Discussion & conclusion

Although no continuous $\delta^{13}C\text{-}CH_4$ observed time-series are available yet, inverse modelers have been considering $\delta^{13}C\text{-}CH_4$ observations as promising to distinguish methane sources for a while (e.g. Hein et al. 1997). The assimilation of $\delta^{13}C\text{-}CH_4$ flask data into 3D-chemistry-transport global models has shown small changes in the balance of sources, involving mostly biomass burning at the global scale (Bousquet et al., 2006, see their supplementary page 7). This modest impact was explained by the scarcity of $\delta^{13}C\text{-}CH_4$ observations (only 13 flask stations in Bousquet et al., 2006), and the uncertainties on isotopic signatures. Since then the former has slightly improved at the global scale (20 flask sites reported in the World Data Center for Greenhouse Gases database at present; gaw.kishou.go.jp/) and continuous measurements are expected (e.g. Thornton et al., 2016b) but the latter is still an issue because it is necessary to obtain precise isotopic signatures at the regional scale for the various processes emitting methane. 3D atmospheric forward modeling has also been used to interpret methane changes of the past decades through scenarios of methane emissions, methane sinks, and isotopic signatures (Monteil et al., 2011; Warwick et al., 2016), demonstrating the added-value of the global monitoring of methane isotopes, although the above limitations are still present. Taking into account these limitations, most recent inverse studies integrating $\delta^{13}C\text{-}CH_4$ data have only represented atmospheric transport with simple box-models and, therefore, have assimilated hemispheric or global mean time-series of ^{13}C observations (e.g., Shaefer et al., 2016, Turner et al., 2017; Schwieztke et al., 2016). Such studies use strong simplifications in their setup and can obviously only address hemispheric to global scale emissions and trends.

Our work aims at preparing 3D inversions assimilating future continuous $\delta^{13}C\text{-}CH_4$ time-series to address the reduction of uncertainties on methane emissions at the regional scale. The Arctic region was chosen to make this first analysis because it is a climate-sensitive region (with potentially larger methane sources than today in the context of a changing climate) and because the mix of methane sources is less complicated than in the tropics. Even in this apparently favorable context, the situation of the detectability of methane sources using $\delta^{13}C\text{-}CH_4$ observations is found challenging for at least three reasons. First, as already noted in Thonat et al. (2017), most of the methane signals received at Arctic stations at the synoptic to seasonal scales come from lower latitudes outside the Arctic domain, thus limiting the expected signal to noise ratio of the Arctic sources. Second, the analysis presented in Sect. 3 reveals that, if isotopic signals from wetland emissions should be detectable at most existing sites with reasonable measurement uncertainties on a daily basis (~0.5‰), detecting other sources would require more challenging measurement uncertainties: typically less than 0.2‰ for freshwaters, less than 0.15‰ for ESAS, less than 0.1‰ for anthropogenic emissions (except at YAK) and less than 0.02‰ for other sources. Such ambitious values require solving or at least monitoring precisely the present drifts of existing instruments and stress the importance of having a precise scale for regular calibration. Third, the vision per source developed here is optimistic as total isotopic signals received at stations may cancel each other out for some events, thus reducing the number of useful events constraining individual sources. The sensitivity tests, with varying isotopic signatures, do not change the main conclusions on the detectability of methane emissions.

Next steps of this work involve i) the deployment of at least one $\delta^{13}C\text{-}CH_4$ instrument to acquire real observations, ii) the refinement of isotopic signatures of the various emissions at the regional scale, and iii) the implementation of $\delta^{13}C\text{-}CH_4$ in inversion schemes in order to estimate the potential (if only pseudo continuous data were available) or the real impact of $\delta^{13}C\text{-}CH_4$ to improve the estimation of the regional methane emissions by 3D atmospheric inversions.

Competing interests.
The authors declare that they have no conflict of interest.

Acknowledgements.
The authors acknowledge the principal investigators, Bruce Vaughn, James White and Sylvia Michel, of the five observation sites measuring $^{13}CH_4$ in the Arctic regions, whose data were used in this study, for maintaining methane measurements at high latitudes and sharing their data through the World Data Center for Greenhouse Gases (WDCGG). This work has been supported by the Franco-Swedish IZOMET-FS "Distinguishing Arctic CH_4 sources to the atmosphere using inverse analysis of high-frequency CH_4, $^{13}CH_4$ and CH_3D measurements" project. The study extensively relies on the meteorological data provided by the ECMWF. Calculations were performed using the computing resources of LSCE, maintained by François Marabelle and the LSCE IT team.

References

Aben, R. C. H., Barros, N., van Donk, E., Frenken, T., Hilt, S., Kazanjian, G., Lamers, L. P. M., Peeters, E. T. H. M., Roelofs, J. G. M., de Senerpont Domis, L., Stephan, S. Velthuis, M., Van de Waal, D. B., Wik, M., Thornton, B. F., Wilkinson, J., DelSontro, T., and Kosten, S.: Cross continental increase in methane ebullition under climate change, Nature Commun., 8, 1682, https://doi.org/10.1038/s41467-017-01535-y, 2017.

Bastviken, D., Tranvik, L. J., Downing, J. A., Crill, P. M., and Enrich-Prast, A.: Freshwater methane emissions offset the continental carbon sink, Science, 331, 50, https://doi.org/10.1126/science.1196808, 2011.

Berchet, A., Pison, I., Chevallier, F., Paris, J.-D., Bousquet, P., Bonne, J.-L., Arshinov, M. Y., Belan, B. D., Cressot, C., Davydov, D. K., Dlugokencky, E. J., Fofonov, A. V., Galanin, A., Lavrič, J., Machida, T., Parker, R., Sasakawa, M., Spahni, R., Stocker, B. D., and Winderlich, J.: Natural and anthropogenic methane fluxes in Eurasia: a mesoscale quantification by generalized atmospheric inversion, Biogeosciences, 12, 5393-5414, https://doi.org/10.5194/bg-12-5393-2015, 2015.

Berchet, A., Bousquet, P., Pison, I., Locatelli, R., Chevallier, F., Paris, J.-D., Dlugokencky, E. J., Laurila, T., Hatakka, J., Viisanen, Y., Worthy, D. E. J., Nisbet, E., Fisher, R., France, J., Lowry, D., Ivakhov, V. and Hermansen, O.: Atmospheric constraints on the methane emissions from the East Siberian Shelf, Atmos. Chem. Phys., 16(6), 4147-4157, https://doi.org/10.5194/acp-16-4147-2016, 2016.

Bergamaschi, P., Lubina, C., Königstedt, R., Fischer, H., Veltkamp, A. C., and Zwaagstra, O.: Stable isotopic signatures (δ13C, δD) of methane from European landfill sites, J. Geophys. Res., 103, 8251-8265, https://doi.org/10.1029/98JD00105, 1998.

Bernard, S.: Evolution temporelle du méthane et du protoxyde d'azote dans l'atmosphère : contrainte par l'analyse de leurs isotopes stables dans le névé et la glace polaires, PhD dissertation, Univ. Grenoble 1, https://tel.archives-ouvertes.fr/tel-00701325, 2004.

Bilek, R. S., Tyler, S. C., Kurihara, M., and Yagi, K.: Investigation of cattle methane production and emission over a 24-hour period using measurements of δ13C and δD of emitted CH4 and rumen water, J. Geophys. Res., 106, 15405-15413, https://doi.org/10.1029/2001JD900177, 2001.

Bohn, T. J., Melton, J. R., Ito, A., Kleinen, T., Spahni, R., Stocker, B. D., Zhang, B., Zhu, X., Schroeder, R., Glagolev, M. V., Maksyutov, S., Brovkin, V., Chen, G., Denisov, S. N., Eliseev, A. V., Gallego-Sala, A., McDonald, K. C., Rawlins, M. A., Riley, W. J., Subin, Z. M., Tian, H., Zhuang, Q., and Kaplan, J. O.: WETCHIMP-WSL: intercomparison of wetland methane emissions models over West Siberia, Biogeosciences, 12, 3321-3349, https://doi.org/10.5194/bg-12-3321-2015, 2015.

Bouchard, F., Laurion, I., Preskienis, V., Fortier, D., Xu, X., and Whiticar, M. J.: Modern to millennium-old greenhouse gases emitted from ponds and lakes of the Eastern Canadian Arctic (Bylot Island, Nunavut), Biogeosciences, 12, 7279–7298, https://doi.org/10.5194/bg-12-7279-2015, 2015.

Bousquet, P., Ciais, P., Miller, J., Dlugokencky, E., Hauglustaine, D., Prigent, C., Van der Werf, G., Peylin, P., Brunke, E.-G., and Carouge, C.: Contribution of anthropogenic and natural sources to atmospheric methane variability, Nature, 443, 439–443, 2006.

Bousquet, P., Ringeval, B., Pison, I., Dlugokencky, E. J., Brunke, E.- G., Carouge, C., Chevallier, F., Fortems-Cheiney, A., Frankenberg, C., Hauglustaine, D. A., Krummel, P. B., Langenfelds, R. L., Ramonet, M., Schmidt, M., Steele, L. P., Szopa, S., Yver, C., Viovy, N., and Ciais, P.: Source attribution of the changes in atmospheric methane for 2006–2008, Atmos. Chem. Phys., 11, 3689–3700, https://doi.org/10.5194/acp-11-3689-2011, 2011.

Brosius, L. S., Walter Anthony, K. M., Grosse, G., Chanton, J. P., Farquharson, L. M., Overduin, P. P., and Meyer, H.: Using the deuterium isotope composition of permafrost meltwater to constrain thermokarst lake contributions to atmospheric CH4 during the last deglaciation, J. Geophys. Res., 117, G01022, https://doi.org/10.1029/2011JG001810, 2012.

Brunskill, G. J., Burns, K. A., and Zagorskis, I.: Natural flux of greenhouse methane from the Timor Sea to the atmosphere, J. Geophys. Res., 116, G02024, https://doi.org/10.1029/2010JG001444, 2011.

Burkholder, J. B., Sander, S. P., Abbatt, J., Barker, J. R., Huie, R. E., Kolb, C. E., Kurylo, M. J., Orkin, V. L., Wilmouth, D. M., and Wine, P. H.: Chemical Kinetics and Photochemical Data for Use in Atmospheric Studies, Evaluation No. 18, JPL Publication 15-10, Jet Propulsion Laboratory, Pasadena, 2015.

Ciais, P., et al., Carbon and Other Biogeochemical Cycles. In: Climate Change 2013: The Physical Science Basis. Contribution of Working Group I to the Fifth Assessment Report of the Intergovernmental Panel on Climate Change.*Rep.*, Cambridge University Press, Cambridge, United Kingdom and New York, NY, USA, 2013.

Chanton, J. P., Rutkowski, C. M., and Mosher, B.: Quantifying methane oxidation from landfills using stable isotope analysis of downwind plumes, Envir. Sci. Tech., 33, 3755-3760, https://doi.org/10.1021/es9904033, 1999.

Chanton, J. P., Rutkowski, C. M., Schwartz, C. C., Ward, D. E., and Boring, L.: Factors influencing the stable carbon isotopic signature of methane from combustion and biomass burning, J. Geophys. Res., 105, 1867-1877, https://doi.org/10.1029/1999JD900909, 2000.

Chasar, L. S., Chanton, J. P., Glaser, P. H., and Siegel, D. I.: Methane concentration and stable isotope distribution as evidence of rhizospheric processes: comparison of a fen and bog in the glacial lake Agassiz peatland complex, Ann. Bot., 86, 655-663, https://doi.org/10.1006/anbo.2000.1172, 2000.

Craig, H.: Isotopic standards for carbon and oxygen and correction factors for mass spectrometric analysis of carbon dioxide, Geochim. Cosmochim. Ac., 12, 133– 149, 1957.

Dlugokencky, E. J., Nisbet, E. G., Fisher, R., and Lowry, D.: Global atmospheric methane: budget, changes and dangers, Philos. T. Roy. Soc. A, 369, 2058–2072, https://doi.org/10.1098/rsta.2010.0341, 2011.

Dmitrenko, I. A., Kirillov, S. A., Tremblay, L. B., Kassens, H., Anisimov, O. A., Lavrov, S. A., Razumov, S. O., and Grigoriev, M. N.: Recent changes in shelf hydrography in the Siberian Arctic: Potential for subsea permafrost instability, J. Geophys. Res., 116, C10027, https://doi.org/10.1029/2011JC007218, 2011.

Etiope, G.: Natural emissions of geological methane in Europe, Atmos. Environ., 43, 1430-1443, https://doi.org/10.1016/j.atmosenv.2008.03.014, 2009

Etiope, G.: Natural gas seepage. The Earth's hydrocarbon degassing, Springer International Publishing, https://doi.org/10.1007/978-3-319-14601-0, Switzerland, 2015.

Fisher, R. E., : Arctic methane sources: Isotopic evidence for atmospheric inputs, Geophys. Res. Lett., 38, L21803, https://doi.org/10.1029/2011GL049319, 2011.

Fisher, R. E., France, J. L., Lowry, D., Lanoisellé, M., Brownlow, R., Pyle, J. A., Cain, M., Warwick, N., Skiba, U. M., Drewer, J., Dinsmore, K. J., Leeson, S. R., Bauguitte, S. J.-B., Wellpott, A., O'Shea, S. J., Allen, G., Gallagher, M. W., Pitt, J., Percival, C. J., Bower, K., George, C., Hayman, G. D., Aalto, T., Lohila, A., Aurela, M., Laurila, T., Crill, P. M., McCalley, C. K., and Nisbet, E. G.: Measurements of the 13C isotopic signature of methane emissions from northern European wetlands, G. Biogeochem. Cy., 31, 605-623, https://doi.org/10.1002/2016GB005504, 2017

France, J. L., Cain, M., Fisher, R. E., Lowry, D., Allen, G., O'Shea, S. J., Illingworth, S., Pyle, J., Warwick, N., Jones, B. T., Gallagher, M. W., Bower, K., Le Breton, M., Percival, C., Muller, J., Bauguitte, S., George, C., Hayman, G. D., Manning, A. J., Lund Myhre, C., Lanoisellé, M., and Nisbet, E. G.: Measurements of δ13C in CH4 and using particle dispersion modeling to characterize sources of Arctic methane within an air mass, J. Geophys. Res., 121, 14,257–14,270, doi:10.1002/2016JD026006, 2016.

Galand, P. E., Yrjälä, K., and Conrad, R.: Stable carbon isotope fractionation during methanogenesis in three boreal peatland ecosystems, Biogeosciences, 7, 3893-3900, https://doi.org/10.5194/bg-7-3893-2010, 2010

Giglio, L., Randerson, J. T., and van der werf, G.: Analysis of daily, monthly, and annual burned area using the fourth-generation global fire emissions database (GFED4), J. Geophys. Res., 118, 317-328, https://doi.org/10.1002/jgrg.20042, 2013.

Atmos. Chem. Phys. Discuss., https://doi.org/10.5194/acp-2018-1217
Manuscript under review for journal Atmos. Chem. Phys.
Discussion started: 26 November 2018

Atmospheric Chemistry and Physics
Discussions

Hourdin, F., Musat, I., Bony, S. et al. Clim Dyn (2006) 27: 787. https://doi.org/10.1007/s00382-006-0158-0

Houweling, S., Röckmann, T., Aben, I., Keppler, F., Krol, M., Meirink, J. F., Dlugokencky, E. J., and Frankenberg, C.: Atmospheric constraints on global emissions of methane from plants, Geophys. Res. Let., 33, L15821, https://doi.org/10.1029/2006GL026162, 2006

Klevenhusen, F., Bernasconi, S. M., Kreuzer, M., and Soliva, C. : Experimental validation of the Intergovernmental Panel on Climate Change default values for ruminant-derived methane and its carbon-isotope signature, Animal Production Science, 50, https://doi/org/10.1071/AN09112, 2010.

Lassey, K. R., Etheridge, D. M., Lowe, D. C., Smith, A. M., and Ferretti, D. F.: Centennial evolution of the atmospheric methane budget: what do the carbon isotopes tell us?, Atmos. Chem. Phys., 7, 2119-2139, https://doi.org/10.5194/acp-7-2119-2007, 2007.

Lehner, B., and Döll, P.: Development and validation of a global database of lakes, reservoirs and wetlands, J. Hydrol., 296, 1-22, https://doi.org/10.1016/j.jhydrol.2004.03.028, 2004.

Levin, I., Glatzel-Mattheier, H., Marik, T., Cuntz, M., and Schmidt, M.: Verification of German methane emission inventories and their recent changes based on atmospheric observations, J. Geophys. Res., 104, 3447-3456, https://doi.org/10.1029/1998JD100064, 1999.

McCalley, C. K., Woodcroft, B. J., Hodgkins, S. B., Wehr, R. A., Kim, E.-H., Mondav, R., Crill, P. M., Chanton, J. P., Rich, V. I., Tyson, G. W., and Saleska, S. R.: Methane dynamics regulated by microbial community response to permafrost thaw, Nature, 514, 478–481, https://doi.org/10.1038/nature13798, 2014.

McManus, J. B., D. D. Nelson, and M. S. Zahniser, Long-term continuous sampling of $^{12}CO_2$, $^{13}CO_2$ and $^{12}C^{18}O^{16}O$ in ambient air with a quantum cascade laser spectrometer, Isotopes Environ. Health Stud., 46(1), 49–63, doi:10.1080/10256011003661326, 2010.

McNorton, J., Gloor, E., Wilson, C., Hayman, G. D., Gedney, N., Comyn-Platt, E., Marthews, T., Parker, R. J., Boesch, H., and Chipperfield, M. P.: Role of regional wetland emissions in atmospheric methane variability, Geophys. Res. Lett., 43, 11,433-11,444, https://doi.org/10.1002/2016GL070649, 2016.

Menut, L., Bessagnet, B., Khvorostyanov, D., Beekmann, M., Blond, N., Colette, A., Coll, I., Curci, G., Foret, G., Hodzic, A., Mailler, S., Meleux, F., Monge, J.-L., Pison, I., Siour, G., Turquety, S., Valari, M., Vautard, R., and Vivanco, M. G.: CHIMERE 2013: a model for regional atmospheric composition modelling, Geosci. Model Dev., 6, 981–1028, https://doi.org/10.5194/gmd-6-981-2013, 2013.

Mikaloff Fletcher, S. E. M., Tans, P. P. , Bruhwiler, L. M. , Miller, J. B. ,and Heimann, M. : CH4 sources estimated from atmospheric observations of CH4 and its C-13/C-12 isotopic ratios: 1. Inverse modeling of source processes, Global. Biogeochem. Cycles, 18(4), GB4004, https://doi/org/4010.1029/2004GB002223, 2004.

Monteil, G., Houweling, S., Dlugockenky, E. J., Mænhout, G., Vaughn, B. H., White, J. W. C., and Rockmann, T.: Interpreting methane variations in the past two decades using measurements of CH4 mixing ratio and isotopic composition, Atmos. Chem. Phys., 11, 9141–9153, https://doi.org/10.5194/acp-11-9141-2011, 2011.

Myhre, C. L., et al. : Extensive release of methane from Arctic seabed west of Svalbard during summer 2014 does not influence the atmosphere, Geophys. Res. Lett., 43, 4624–4631, https://doi.org/10.1002/2016GL068999, 2016.

Nelson, D. D., B. McManus, S. Urbanski, S. Herndon, and M. S. Zahniser, High precision measurements of atmospheric nitrous oxide and methane using thermoelectrically cooled mid-infrared quantum cascade lasers and detectors, Spectrochim. Acta, Part A, 60(14), 3325–3335, doi:10.1016/j.saa.2004.01.033, 2004.

Nisbet, E. G., Dlugokencky, E. J., Manning, M. R., Lowry, D., Fisher, R. E., France, J. L., Michel, S. E., Miller, J. B., White, J. W. C., Vaughn, B., Bousquet, P., Pyle, J. A., Warwick, N. J., Cain, M., Brwnlow, R., Zazzeri, G., Lanoisellé, M., Manning, A. C., Gloor, E., Worthy, D. E. J., Brunke, E.-G., Labuschagne, C., Wolff, E. W., and Ganesan, A. L.: Rising atmospheric methane: 2007-2014 growth and isotopic shift, Global Biogeochem. Cy., 30, 1356-1370, https://doi.org/10.1002/2016GB005406, 2016.

O'Shea, S. J., Allen, G., Gallagher, M. W., Bower, K., Illingworth, S. M., Muller, J. B. A., Jones, B. T., Percival, C. J., Bauguitte, S. J.-B., Cain, M., Warwick, N., Quiquet, A., Skiba, U., Drewer, J., Dinsmore, K., Nisbet, E. G., Lowry, D., Fisher, R. E., France, J. L., Aurela, M., Lohila, A., Hayman, G., George, C., Clark, D. B., Manning, A. J., and Pyle, J.: Methane and carbon dioxide fluxes and their regional scalability for the European Arctic wetlands during the MAMM project in summer 2012, Atmos. Cehm. Phys., 14, 13159-13174, https://doi.org/10.5194/acp-14-13159-2014, 2014

Olivier, J., and Janssens-Maenhout, G.: Part III: Greenhouse gas emissions, III.1-III.51, in: CO2 emissions from fuel combustion, 2012 Edition, International Energy Agency (IEA), Paris, 2012.

Overduin, P. P., Liebner, S., Knoblauch, C., Günther, F., Wetterich, S., Schirrmeister, L., Hubberten, H.-W., and Grigoriev, M. N.: Methane oxidation following submarine permafrost degradation: Measurements from a central Laptev Sea shelf borehole, J. Geophys. Res., 120, 965–978, https://doi.org/10.1002/2014JG002862, 2015.

Pisso, I., et al. (2016), Constraints on oceanic methane emissions west of Svalbard from atmospheric in situ measurements and Lagrangian transport modeling, J. Geophys. Res. Atmos., 121, 14, 188–14, 200, doi:10.1002/2016JD025590.

Podbaronova, J.: Assessment of coals fro Russia and countries of former Soviet Union for utility fluidized bed boilers, Master's thesis, Lappeenranta University of Technology, Faculty of Technology, Bioenergy Technology, 2010.

Rice, D. D.: Composition and origins of coalbed gas: Hydrocarbons from coal, AAPG Studies in Geology, 38, 159–184, 1993.

Ridgwell, A. J., Marshall, S. J., and Gregson, K.: Consumption of atmospheric methane by soils: a process-based model, Global Biogeochem. Cy., 13, 59-70, 1999.

Rigby, M., Manning, A. J., and Prinn, R. G.: The value of high-frequency, high-precision methane isotopologue measurements for source and sink estimation, J. Geophys. Res.-atmos., 117, 2012.

Ringeval, B., de Noblet-Ducoudré, N., Ciais, P., Bousquet, P., Prigent, C., Papa, F., and Rossow, W. B.: An attempt to quantify the impact of changes in wetland extent on methane emissions on the seasonal and interannual time scales, Global Biogeochem. Cy., 24(2), 1–12, https://doi.org/10.1029/2008GB003354, 2010.

Ringeval, B., Friedlingstein, P., Koven, C., Ciais, P., de Noblet-Ducoudré, N., Decharme, B., and Cadule, P.: Climate-CH4 feedback from wetlands and its interaction with the climate-CO2 feedback, Biogeosciences, 8, 2137-2157, https://doi.org/10.5194/bg-8-2137-2011, 2011.

Ruppel, C.: Permafrost-Associated Gas Hydrate: Is It Really Approximately 1 % of the Global System, or: Special Issue in honor of E. Dendy Sloan on the occasion of his 70th Birthday, Journal of Chemical & Engineering Data, 60, 429-436; https://doi.org/ 10.1021/je500770m, 2015.

Santoni, G. W., B. H. Lee, J. P. Goodrich, R. K. Varner, P. M. Crill, J. B. McManus, D. D. Nelson, M. S. Zahniser, and S. C. Wofsy (2012), Mass fluxes and isofluxes of methane (CH4) at a New Hampshire fen measured by a continuous wave quantum cascade laser spectrometer, J. Geophys. Res., 117, D10301, doi:10.1029/2011JD016960.

Sapart, C. J., Shakhova, N., Semiletov, I., Jansen, J., Szidat, S., Kosmach, D., Dudarev, O., van der Veen, C., Egger, M., Sergienko, V., Salyuk, A., Tumskoy, V., Tison, J.-L., and Röckmann, T.: The origin of methane in the East Siberian Arctic Shelf unraveled with triple isotope analysis, Biogeosciences, 14, 2283-2292, https://doi.org/10.5194/bg-14-2283-2017, 2017.

Saunois, M., Bousquet, P., Poulter, B., Peregon, A., Ciais, P., Canadell, J. G., Dlugokencky, E. J., Etiope, G., Bastviken, D., Houweling, S., Janssens-Maenhout, G., Tubiello, F. N., Castaldi, S., Jackson, R. B., Alexe, M., Arora, V. K., Beerling, D. J., Bergamaschi, P., Blake, D. R., Brailsford, G., Brovkin, V., Bruhwiler, L., Crevoisier, C., Crill, P., Curry, C., Frankenberg, C., Gedney, N., Höglund-Isaksson, L., Ishizawa, M., Ito, A., Joos, F., Kim, H.-S., Kleinen, T., Krummel, P., Lamarque, J.-F., Langenfelds, R., Locatelli, R., Machida, T., Maksyutov, S., McDonald, K. C., Marshall, J., Melton, J. R., Morino, I., O'Doherty, S., Parmentier, F.-J. W., Patra, P. K., Peng, C., Peng, S., Peters, G. P., Pison, I., Prigent, C., Prinn, R., Ramonet, M., Riley, W. J., Saito, M., Schroeder, R., Simpson, I. J., Spahni, R., Steele, P., Takizawa, A., Thornton, B. F., Tian, H., Tohjima, Y., Viovy, N., Voulgarakis, A., van Weele, M., van der Werf, G., Weiss, R., Wiedinmyer, C., Wilton, D. J., Wiltshire, A., Worthy, D., Wunch, D. B., Xu, X., Yoshida, Y., Zhang, B., Zhang, Z. and Zhu, Q.: The Global Methane Budget 2000–2012, Earth Syst. Sci. Data, 8, 697-751, https://doi.org/10.5194/essd-8-697-2016, 2016 .

Saunois, M., Bousquet, P., Poulter, B., Peregon, A., Ciais, P., Canadell, J. G., Dlugokencky, E. J., Etiope, G., Bastviken, D., Houweling, S., Janssens-Maenhout, G., Tubiello, F. N., Castaldi, S., Jackson, R. B., Alexe, M., Arora, V. K., Beerling, D. J., Bergamaschi, P., Blake, D. R., Brailsford, G., Bruhwiler, L., Crevoisier, C., Crill, P., Covey, K., Frankenberg, C., Gedney, N., Höglund-Isaksson, L., Ishizawa, M., Ito, A., Joos, F., Kim, H.-S., Kleinen, T., Krummel, P., Lamarque, J.-F., Langenfelds, R., Locatelli, R., Machida, T., Maksyutov, S., Melton, J. R., Morino, I., Naik, V., O'Doherty, S., Parmentier, F.-J. W., Patra, P. K., Peng, C., Peng, S., Peters, G. P., Pison, I., Prinn, R., Ramonet, M., Riley, W. J., Saito, M., Santini, M., Schroeder, R., Simpson, I. J., Spahni, R., Takizawa, A., Thornton, B. F., Tian, H., Tohjima, Y., Viovy, N., Voulgarakis, A., Weiss, R., Wilton, D. J., Wiltshire, A., Worthy, D., Wunch, D., Xu, X., Yoshida, Y., Zhang, B., Zhang, Z., and Zhu, Q.: Variability and quasi-decadal changes in the methane budget over the period 2000–2012, Atmos. Chem. Phys., 17, 11135-11161, https://doi.org/10.5194/acp-17-11135-2017, 2017.

Schaefer, H., Fletcher, S. E., Veidt, C., Lassey, K. R., Brailsford, G. W., Bromley, T. M., Dlugokencky, E. J., Michel, S. E., Miller, J. B., Levin, I., Lowe, D. C., Martin, R. J., Vaughn, B. H. and White, J. W.: A 21st century shift from fossil-fuel to biogenic methane emissions indicated by 13CH4, Science, https://doi.org/10.1126/science.aad2705, 2016.

Schoell, M.: The hydrogen and carbon isotopic composition of methane from natural gases of various origins, Geochim. Cosmochim. Ac., 44, 649-661, 1980.

Schuur, E. A. G., McGuire, A. D., Schädel, C., Grosse, G., Harden, J. W., Hayes, D. J., Hugelius, G., Koven, C. D., Kuhry, P., Lawrence, D. M., Natali, S. M., Olefeldt, D., Romanovsky, V. E., Schaefer, K., Turetsky, M. R., Treat, C. C., and Vonk, J. E.: Climate change and the permafrost carbon feedback, Nature, 520, 171-179, https://doi.org/10.1038/nature14338, 2015.

Schwietzke, S., Sherwood, O. A., Bruhwiler, L. M. P., Miller, J. B., Etiope, G., Dlugokencky, E. J., Michel, S. E., Arling, V. A., Vaughn, B. H., White, J. W. C., and Tans, P. P.: Upward revision of global fossil fuel methane emissions based on isotope database, Nature, 58, 88-91, https://doi.org/10.1038/nature19797, 2016.

Shakhova, N., Semiletov, I., Salyuk, A., Yusupov, V., Kosmach, D., and Gustafsson, O.: Extensive Methane Venting to the Atmosphere from Sediments of the East Siberian Arctic Shelf, Science, 327, 1246–1250, https://doi.org/10.1126/science.1182221, 2010.

Shakhova, N., Semiletov, I., Leifer, I., Sergienko, V., Salyuk, A., Kosmach, D., Chernykh, D., Stubbs, C., Nicolsky, D., Tumskoy, V., and Gustafsson, Ö.: Ebullition and storm-induced methane release from the East Siberian Arctic Shelf, Nat. Geosci., 7, 64–70, https://doi.org/10.1038/ngeo2007, 2014.

Sherwood, O. A., Schwietzke, S., Arling, V. A., and Etiope, G.: Global inventory of gas geochemistry data from fossil fuel, microbial and biomass burning sources, version 2017, Earth Syst. Sci. Data., 9, 639-656, https://doi.org/10.5194/essd-9-639-2017, 2017.

Sriskantharajah, S., Fisher, R. E., Lowry, D., Aalto, T., Hatakka, J., Aurela, M., Laurila, T., Lohila, A., Kuitunen, E., and Nisbet, E. G.: Stable carbon isotope signatures of methane from a Finnish subarctic wetland, Tellus B, 64, 18818, https://doi.org/10.3402/tellusb.v64i0.18818, 2012.

Sweeney, C., Dlugokencky, E., Miller, C. E., Wofsy, S., Karion, A., Dinardo, S., Chang, R. Y.-W., Miller, J. B., Bruhwiler, L., Crotwell, A. M., Newberger, T., McKain, K., Stone, R. S., Wolter, S. E., Lang, P. E., and Tans, P.: No significant increase in long-term CH4 emissions on North Slope of Alaska despite significant increase in air temperature, Geophys. Res. Lett., 43, 6604-6611, https://doi.org/10.1002/2016GL069292, 2016.

Tan, Z. and Zhuang, Q.: Arctic lakes are continuous methane sources to the atmosphere under global warming, Environ. Res. Lett., 10, 054016, https://doi.org/10.1088/1748-9326/10/5/054016, 2015a.

Tans, P. P.: A note on isotopic ratios and the global atmospheric methane budget, Global. Biogeochem. Cycles, 11(1), 77-81, https://doi.org/10.1029/96GB03940, 1997.

Thompson, H. A, White, J. R., Pratt, L. M., and Sauer, P. E.: Spatial variation in flux, δ13C and δ2H of methane in a small Arctic lake with fringing wetland in western Greenland, Biogeochemistry, 131, 17-33, https://doi.org/10.1007/s10533-016-0261-1, 2016.

Thompson, R. L., Sasakawa, M., Machida, T., Aalto, T., Worthy, D., Lavric, J. V., Lund Myhre, C., and Stohl, A.: Methane fluxes in the high northern latitudes for 2005–2013 estimated using a Bayesian atmospheric inversion, Atmos. Chem. Phys., 17, 3553-3572, https://doi.org/10.5194/acp-17-3553-2017, 2017.

Thonat, T., Saunois, M., Bousquet, P., Pison, I., Tan, Z., Zhuang, Q., Crill, P. M., Thornton, B. F., Bastviken, D., Dlugokencky, E. J., Zimov, N., Laurila, T., Hatakka, J., Hermansen, O., and Worthy, D. E. J.: Detectability of Arctic methane sources at six sites performing continuous atmospheric measurements, Atmos. Chem. Phys., 17, 8371–8394, https://doi.org/10.5194/acp-17-8371-2017, 2017.

Thornton, B. F., Geibel, M. C., Crill, P. M., Humborg, C., and Mörth, C.-M.: Methane fluxes from the sea to the atmosphere across the Siberian shelf seas, Geophys. Res. Lett., 43, https://doi.org/10.1002/2016GL068977, 2016a.

Thornton, B. F., Wik, M., and Crill, P. M.: Double-counting challenges the accuracy of high-latitude methane inventories, Geophys. Res. Lett., 43, 12,569-12,577, https://doi.org/10.1002/2016GL071772, 2016b.

Tyler, S. C., Rice, A. L. , and Ajie, H. O.:, Stable isotope ratios in atmospheric CH4: Implications for seasonal sources and sinks, J. Geophys. Res.-atmos., 112(D3), 2007.

van der Werf, G. R., Randerson, J. T., Giglio, L., Collatz, G. J., Mu, M., Kasibhatla, P. S., Morton, D. C., DeFries, R. S., Jin, Y., and van Leeuwen, T. T.: Global fire emissions and contribution of deforestation, savanna, forest, agricultural, and peat fires (1997-2009), Atmos. Chem. Phys., 10, 11707-11735, https://doi.org/10.5194/acp-10-11707-2010, 2010.

Vautard, R., Beekmann, M., Roux, J., and Gombert, D.: Validation of a hybrid forecasting system for the ozone concentrations over the Paris area, Atmos. Environ., 35, 2449–2461, https://doi.org/10.1016/S1352-2310(00)00466-0, 2001.

Walter, K. M., Smith, L. C., and Chapin III, F. S.: Methane bubbling from northern lakes: present and future contributions to the global budget, Phil. Trans. R. Soc. A, 365, 1657-1676, https://doi.org/10.1098/rsta.2007.2036, 2007.

Walter, K. M., Chanton, J. P., Chapin, F. S., Schuur, E. A. G., and Zimov, S. A.: Methane production and bubble emissions from arctic lakes: Isotopic implications for source pathways and ages, J. Geophys. Res., 113, G00A8, https://doi.org/10.1029/2007JG000569, 2008.

Walter Anthony, K. M., Anthony, P., Grosse, G., and Chanton, J. P.: Geologic methane seeps along boundaries of Arctic permafrost thaw and melting glaciers, Nat. Geosci., 5, 419-426, htpps://doi.org/10.1038/ngeo1480, 2012.

Warwick, N. J., Cain, M. L., Fisher, R., France, J. L., Lowry, D., Michel, S. E., Nisbet, E. G., Vaughn, B. H., White, J. W. C., and Pyle, J. A.: Using δ13C-CH4 and δD-CH4 to constrain Arctic methane emissions, Atmos. Chem. Phys., 16, 14891-14908, https://doi.org/10.5194/acp-16-14891-2016, 2016.

White, J. W. C., Vaughn, B. H., and Michel, S. E.: University of Colorado, Institute of Arctic and Alpine Research (INSTAAR), Stable Isotopic Composition of Atmospheric Methane (13C) from the NOAA ESRL Carbon Cycle Cooperative Global Air Sampling Network, 1998-2017, Version: 2018-09-24, available at: ftp://aftp.cmdl.noaa.gov/data/trace_gases/ch4c13/flask/, 2018.

Whiticar, M. J.: Carbon and hydrogen isotope systematics of bacterial formation and oxidation of methane, Chem. Geol., 161, 291-314, 1999.

Whiticar, M. and Schaefer, H.: Constraining past global tropospheric methane budgets with carbon and hydrogen isotope ratios in ice, Philos. T. R. Soc. S.-A, 365, 1793-1828, 2007.

Wik, M.: Emission of methane from Northern lakes and ponds, PhD dissertation, Stockholm Univ., 2016.

Wik, M., Varner, R. K., Walter Anthony, K., MacIntyre, S., and Bastviken, D.: Climate-sensitive northern lakes and ponds are critical components of methane release, Nat. Geosci., 9, 99-105, https://doi.org/10.1038/ngeo2578, 2016.

Yamada, K., Ozaki, Y., Nakagawa, F., Sudo, S., Tsuruta, H., and Yoshida, N.: Hydrogen and carbon isotopic measurements of methane from agricultural combustion: Implications for isotopic signatures of global biomass burning sources, J. Geophys. Res., 111, D16306, doi: 10.1029/2005JD006750, 2006.

Zazzeri, G., Lowry, D., Fisher, R. E., France, J. L., Lanoisellé, M., Kelly, B. F. J., Necki, J. M., Iverach, C. P., Ginty, E., Zimnoch, M., Jasek, A., and Nisbet, E. G.: Carbon isotopic signature of coal-derived methane emissions to the atmosphere: from coalification to alteration, Atmos. Chem. Phys., 16, 13669–13680, https://doi.org/10.5194/acp-16-13669-2016, 2016.

Zona, D., Gioli, B., Commane, R., Lindaas, J., Wofsy, S. C., Miller, C. E., Dinardo, S. J., Dengel, S., Sweeney, C., Karion, A., Chang, R. Y.-W., Henderson, J. M., Murphy, P. C., Goodrich, J. P., Moreaux, V., Liljedahl, A., Watts, J. D., Kimball, J. S., Lipson, D. A. and Oechel, W. C.: Cold season emissions dominate the Arctic tundra methane budget, Proc. Natl. Acad. Sci., 113(1), 40-45, https://doi.org/10.1073/pnas.1516017113, 2016.

Atmospheric Chemistry and Physics
Open Access
EGU
Discussions

Table 1. Description of the 24 sites measuring methane used in this study.

Code	Sites	Coordinates	Altitudes (m a.s.l)	$\delta^{13}C\text{-}CH_4$ observations
ALT	Alert	82.45°N, 62.52°W	36	Y
AMB	Ambarchik	69.62°N, 162.30°E	5	-
BKL	Baker Lake	64.17°N, 95.50°W	10	-
BRW	Barrow	71.32°N, 156.60°W	2	Y
BCK	Behchoko	62.80°N, 116.10°W	179	-
CBB	Cambridge Bay	69.10°N, 105.10°W	30	-
CAR	CARVE Tower	65.00°N, 147.60°W	611	-
CHS	Cherskii	68.61°N, 161.34°E	23	-
CHL	Churchill	58.75°N, 94.07°W	9	-
CBA	Cold Bay	55.21°N, 162.72°W	25	Y
DEM	Demyanskoe	59.79°N, 70.87°E	71	-
IGR	Igrim	63.19°N, 64.42°E	53	-
INU	Inuvik	68.30°N, 133.50°E	10	-
KRS	Karasevoe	58.25°N, 82.42°E	78	-
NOY	Noyabrsk	63.43°N, 75.78°E	100	-
PAL	Pallas	67.97°N, 24.12°E	301	-
ICE	Storhofdi	63.40°N, 20.29°W	118	-
SUM	Summit	72.60°N, 38.42°W	3178	Y
TER	Teriberka	69.20°N, 35.10°E	83	-
TIK	Tiksi	71.59°N, 128.92°E	123	-
VGN	Vaganovo	54.50°N, 62.32°E	197	-
YAK	Yakutsk	62.09°N, 129.36°E	198	-
ZEP	Zeppelin	78.91°N, 11.89°E	126	Y
ZOT	Zottino	60.80°N, 89.35°E	104	-

Table 2. Methane emissions and isotopic signatures in the studied domain.

Type of source/sink	Emissions ($TgCH_4\ yr^{-1}$)	$\delta^{13}C\text{-}CH_4$ (‰) / KIE	Variant $\delta^{13}C\text{-}CH_4$ (‰)
Oil and gas	11.9	-46	–
Coal mining	4.7	-55	–
Animals	1.3	-62	–
Landfills	1.1	-52	–
Total anthropogenic	20.5		–
Biomass burning	3.1	-24	–
Geology	4.0	-49	–
ESAS	2.0	-58	-90, -50
Wetlands	29.5	-70	-80, -55
Freshwater systems	9.3	-66	-80, -50
Soil uptake	-3.1	-65.7 / 1.020	–
OH oxidation	–	1.039	–

Table 3. $\delta^{13}C-CH_4$ source signatures reported for wetlands at high northern latitudes.

Measurements location	Type of source	Reference	$\delta^{13}C-CH_4$ (‰)
Manitoba, Canada	Tundra	Wahlen et al. (1989)	-62.9
Ontario, Canada	Wetlands	Kuhlman et al. (1998)	-60.0
Alberta, Canada	Wetlands	Popp et al. (1999)	-66.3 to -63.6
Alaska, USA	Tundra	Quay et al. (1988)	-64
Alaska, USA	Wetlands	Martens et al. (1992)	-65.8
Siberia, Russia	Wetlands	Meth-MonitEUr (2005)	-67.1
Siberia, Russia	Wetlands	Tarasova et al. (2006)	-62.8
Siberia, Russia	Wetlands	Bergamaschi et al. (1998)	-62.4
Siberia, Russia	Wetlands	Sugawara et al. (1996)	-75 to -67
Siberia, Russia	Wetlands (thermokarst basins)	Nakagawa et al. (2002)	-61.1
Northern Fennoscandia	Wetlands	Fisher et al. (2017)	-72.0 to -69.2
Lompolojänkkä, Finland	Wetlands	Sriskantharajah et al. (2012)	-68.7 to -64.9

Table 4. Lowest detectability threshold (in ‰) of Arctic sources at all observation sites in 2012. See Sect. 3.3 for the definition of the detectability threshold.

Station	Anthro-pogenic	Geology	Biomass burning	Wetlands	Fresh-waters	ESAS
ALT	-	-	-	0.2	-	0.02
AMB	-	-	-	0.5	-	0.2
BKL	-	-	-	0.5	0.5	0.02
BRW	-	-	-	0.5	0.05	0.05
BCK	-	-	-	0.5	0.5	0.01
CBB	-	-	-	0.5	0.5	0.02
CAR	-	-	-	0.5	0.01	0.01
CHS	-	-	-	0.5	-	0.015
CHL	-	-	-	0.5	0.1	0.01
CBA	-	-	-	0.2	-	0.01
DEM	0.05	-	-	0.5	0.01	-
IGR	0.05	-	-	0.5	0.02	-
INU	-	-	-	0.5	-	0.02
KRS	0.01	-	-	0.5	-	-
NOY	-	-	-	0.5	-	-
PAL	-	-	-	0.2	0.1	-
ICE	-	-	-	0.15	0.02	-
SUM	-	-	-	0.15	-	-
TER	0.01	-	-	0.2	0.1	-
TIK	-	-	-	0.5	-	0.015
VGN	0.02	-	-	0.2	0.1	-
YAK	0.5	-	-	0.5	-	-
ZEP	-	-	-	0.2	0.01	0.02
ZOT	-	-	-	0.2	-	0.05

Atmos. Chem. Phys. Discuss., https://doi.org/10.5194/acp-2018-1217
Manuscript under review for journal Atmos. Chem. Phys.
Discussion started: 26 November 2018

Atmospheric Chemistry and Physics
Open Access
Discussions

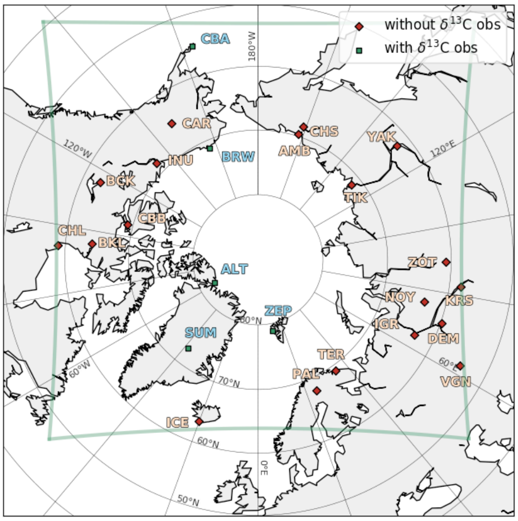

Figure 1. Delimitation of the studied polar domain (green line) and location of the 24 measurement sites used in this study and measuring atmospheric methane. Five stations (blue square) include flask measurements of $\delta^{13}C-CH_4$. The station name acronyms are given in Table 2.

Atmos. Chem. Phys. Discuss., https://doi.org/10.5194/acp-2018-1217
Manuscript under review for journal Atmos. Chem. Phys.
Discussion started: 26 November 2018

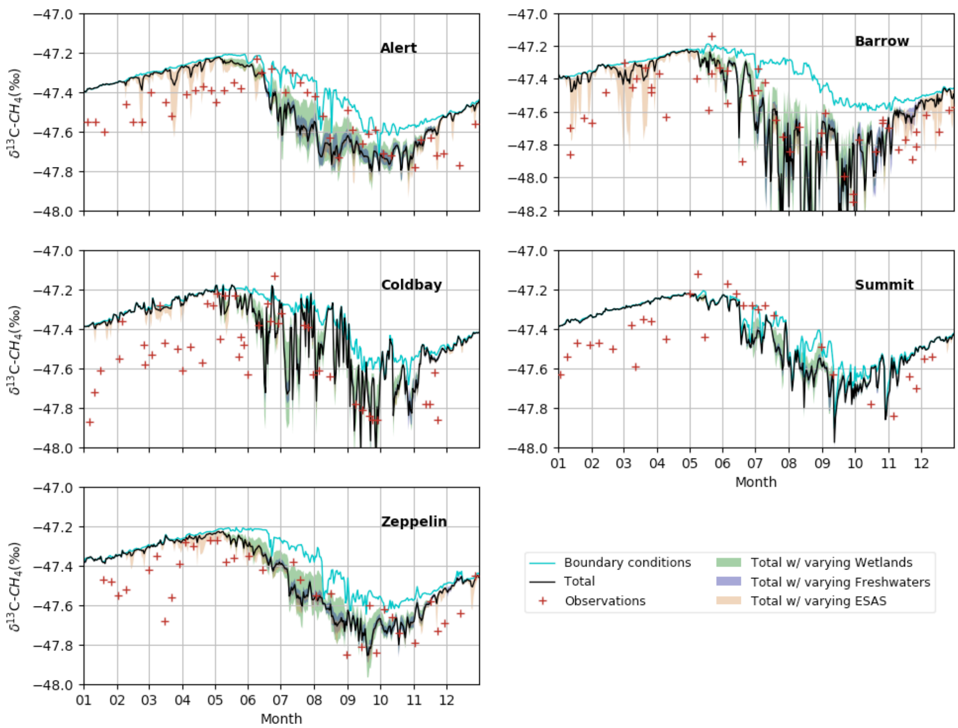

Figure 2. Time series of simulated and observed δ^{13}C-CH_4, at five sites, in 2012. The cyan line represents the contribution of the boundary conditions; the black line represents the total simulated δ^{13}C-CH_4 (boundary conditions + direct contribution of the sources located in the domain); the coloured shades represent total simulated δ^{13}C-CH_4 with varying isotopic signatures for wetlands (green), freshwater systems (blue) and ESAS (orange). The red crosses represent the observations. The hourly-simulated values are averaged into daily values. (Note the different vertical scale for Barrow: the minimum for simulations at Barrow exceeds the chosen scale and reaches -49.3‰.)

Atmos. Chem. Phys. Discuss., https://doi.org/10.5194/acp-2018-1217
Manuscript under review for journal Atmos. Chem. Phys.
Discussion started: 26 November 2018

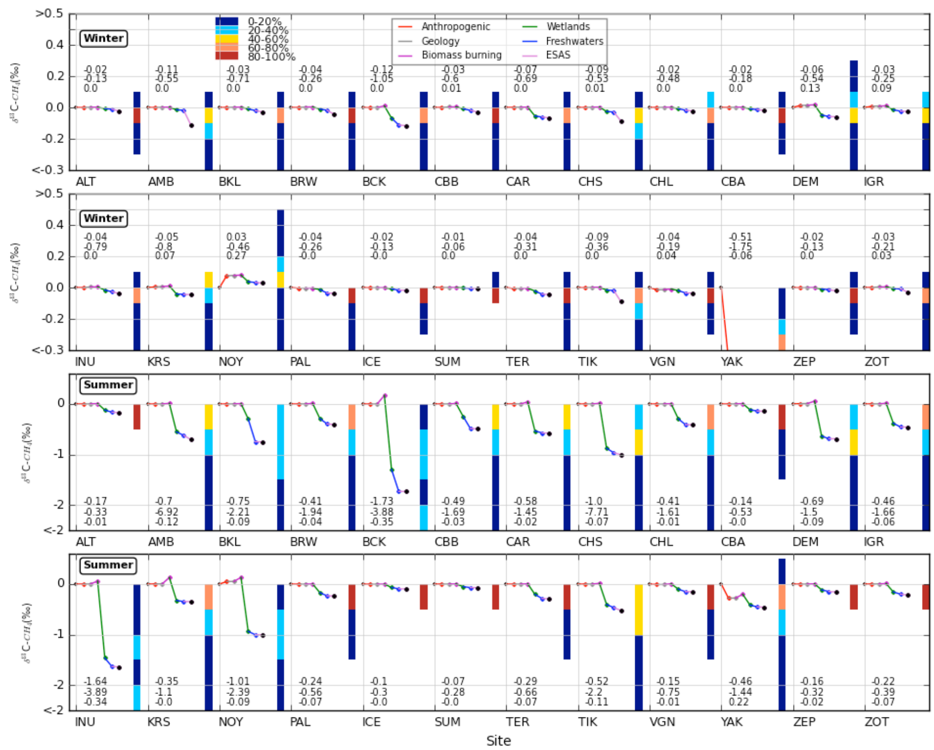

Figure 3.
Winter (top two panels) and summer (bottom two panels) means of the direct contributions of the various Arctic sources to the $\delta^{13}C\text{-}CH_4$ value (in ‰) simulated by CHIMERE at 24 sites in 2012. Bars represent the frequency distribution of daily signatures at each site. See further details in Sect. 2.2.

Atmos. Chem. Phys. Discuss., https://doi.org/10.5194/acp-2018-1217
Manuscript under review for journal Atmos. Chem. Phys.
Discussion started: 26 November 2018

Atmospheric Chemistry and Physics
Open Access
Discussions

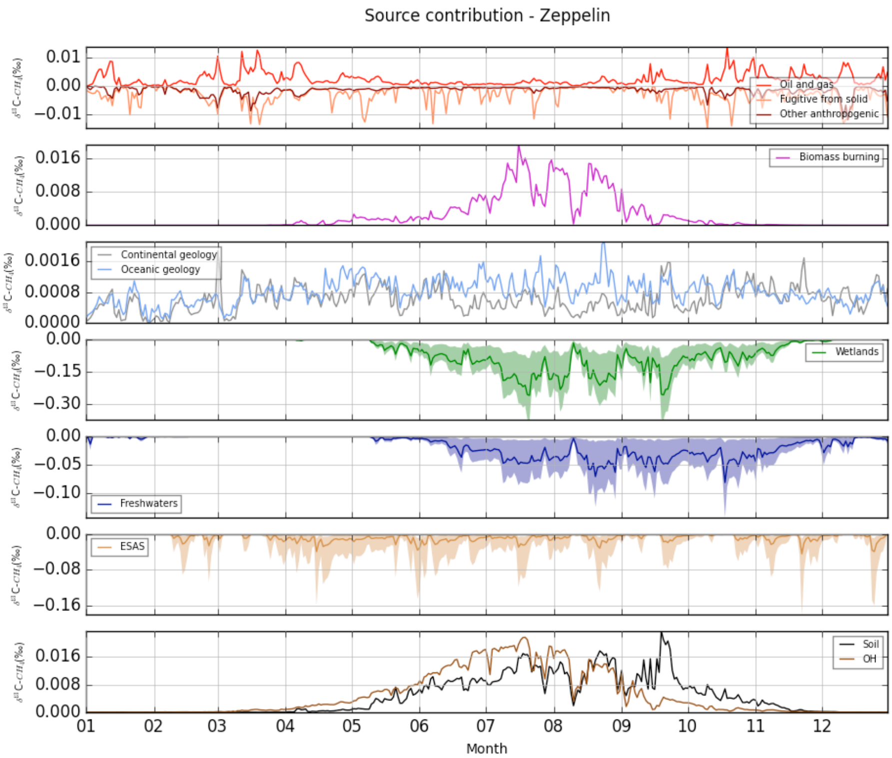

Figure 4. Time series of $\delta^{13}C\text{-}CH_4$ contribution of each source (in ‰), simulated by CHIMERE, in Zeppelin in 2012. The coloured shades represent the range of $\delta^{13}C\text{-}CH_4$ values when varying isotopic signatures. (Note the different scales.)

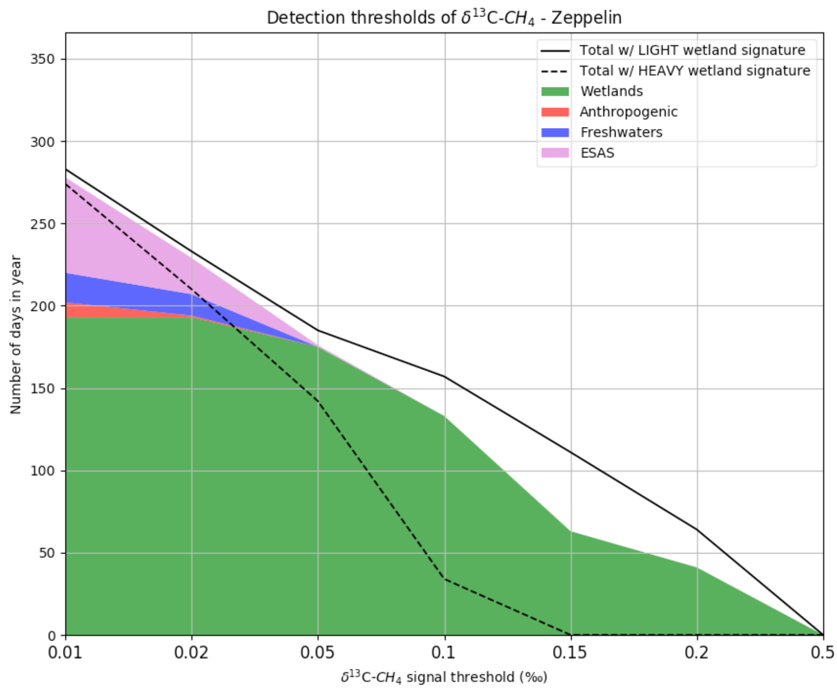

Figure 5. Number of days in 2012 when simulated daily direct contributions of Arctic sources to the $\delta^{13}C\text{-}CH_4$ value are above given thresholds, in Zeppelin. The coloured shades indicate the dominant Arctic source in terms of $\delta^{13}C\text{-}CH_4$ contribution. The plain and dashed black lines represent the total number of days but using various wetland signatures (from the heavier to the lighter scenario). (Note the non-linear scale for the x-axis.)